Biophysical Chemistry, 44 (1992) 47–60
Elsevier Science Publishers B.V., Amsterdam

BIOCHE 01673

Fluorescence decay time distribution for polar dye solutions with time-dependent fluorescent shift

Dmitry M. Gakamsky, Alexander A. Goldin, Eugene P. Petrov and Anatoly N. Rubinov
Institute of Physics, Academy of Sciences of Byelorussia, 220 602 Minsk (Byelorussia)

Abstract

A new method for the recovery of the fluorescence decay time distributions based on the combination of a truncated singular value decomposition and computation of the solution in the presence of non-negative constraints is described. The shape of the fluorescence decay time distribution of polar dye solutions with inhomogeneous broadening of the electronic levels, due to fluctuations of dipole–dipole interactions, was analyzed both theoretically and experimentally. For the first time it has been found that under conditions of single- or double-exponential time-dependent fluorescent shift the distribution is not continuous but consists of discrete peaks. The positions and weights of these peaks are determined by the parameters of the spectral shift. A method for the determination of the dynamic characteristics of the polar region in the membrane bilayer is proposed based on decay time distribution analysis.

Keywords: Decay time distribution; Time-dependent fluorescent shift; Fluorescent probes

1. Introduction

Important advances have been achieved regarding the technique of the fluorescence kinetics processing in recent years. Instead of the common practice to analyze intensity decays by using a sum of discrete exponential decays [1], new methods of recovery of the fluorescence decay time distribution (DTD) have been offered. To date three basic ones have been proposed [2–6] and been widely used [7–21]. They are the maximum entropy (MEM) [3] and the exponential series methods (ESM) [2,4], as well as the method of the recovery of DTD from frequency domain data [5,6]. It has been found [4] that the first two methods are similar in their recovering powers at high level of precision (5 10^5 CPC) of the experimental kinetics. It is also shown that the result of both methods in solving the problem of differentiating the case of a continuous distribution and three discrete components is critically dependent on the separation of the decay times. It was found that for systems with *a priori* continuous distributions both MEM and ESM methods successfully recover DTD shape (e.g., for Förster transfer in rigid media [4,22]). However, the problem of the recovery of DTD even for several chromophores with exponential decays remains

Correspondence to: Dr. D.M. Gakamsky, Institute of Physics, Academy of Sciences of Byelorussia, 220 602 Minsk (Byelorussia).

Abbreviations used in the paper: 3-ANMP–3-amino-*N*-methyl-phthalimide; 1-AN–1-phenylnaphthylamine; 2,6-TNS–2-toluidinonaphthalene-6-sulfonate; IBF–Inhomogeneous broadening function; TDFS–Time-dependent fluorescent shift; DTD–Decay time distribution; and SVD–Singular value decomposition.

ambiguous at the usual data accuracy of commercial fluorometres (5 10^3–5 10^4 CPC) [23]. The application of DTD recovery, to study the fluorescence decay of probes or intrinsic chromophores of the biological samples, can be essentially restricted by the impossibility to improve the experimental accuracy, as the concentration of the chromophores usually is low and amenable to photodegradation. Fluorescence spectra of viscous polar solutions of dyes exhibit considerable spectral–temporal inhomogeneity [24]. It is just the situation that is common for the most probes applied in biochemistry. The inhomogeneous broadening of electronic spectra in such systems leads to a time-dependent fluorescent shift (TDFS). In the case when the spectrum shifts towards the red region (bathochromic shift), an accelerated fluorescence decay takes place at the shorter wavelength side of the emission spectrum (blue slope). In contrast, at the longer wavelength side (red slope) the fluorescence intensity builds up from low values at zero time to a maximum and then decays [25]. A straight forward characterisation of fluorescence kinetics is rather complex, due to the spectral shift, and fluorescence decay cannot be represented as a simple sum of two or three exponentials. To the authors' present knowledge thorough consideration of DTD for the systems with TDFS has not yet been made. However, it has been suggested [5] that the distribution in this case has to be continuous due to the complex behavior of fluorescence spectra.

In general, the spectral shift in polar dye solution as well as in biochemical samples should be a non-exponential one. In the present paper we analyze the case when the spectral shift can be represented as single- or double-exponential.

2. Experimental

Fluorescence decay data were acquired using the time correlated single photon counting technique (PRA-3000). The probes 1-phenylnaphthylamine (1-AN) of chromatographic purity [26] and 2-toluidinonaphthalene-6-sulfonate (2,6-TNS) obtained from Serva (F.R.G.) were used without further purification. 3-ANMP was twice sublimed at $T = 90°C$. Commercial spectral grade glycerol was purified by vacuum distillation and was used to prepare 3-ANMP solutions which had concentration 5 10^{-5} M at the excitation in maximum of the absorption spectrum and 5 10^{-4} M at red-edge excitation.

The experiments were carried out with vesicles obtained by the conventional method from egg-yolk phosphatidylcholine [27]. Vesicles were produced by short-term (10–15 min) sonication of the lipid suspension in 50 mM tris-HCl buffer, pH 7.4, using 150-watts ultrasonic dispergator (MSE). The conditions were chosen such as to provide the predominant formation of bilayer monolamellar vesicles. The separation of the single bilayer vesicles was achieved by means of centrifugation and the additional fractionation on Sepharose 4B. The sizes of vesicles were from 100 to 200 nm. The lipid-to-probe ratio was 500 : 1.

3. Theory

3.1 Method of recovery of decay time distributions

We compute distributions of decay rates $P(\Gamma)$ and then recalculate them to distributions of decay times $P(\tau)$. The recovery of DTD from the experimental kinetics is reduced to solving the Fredholm integral equation of the first kind:

$$I(t) = \int_0^t R(t-t') \int_0^\infty P(\Gamma) \exp(-\Gamma t') \, d\Gamma \, dt', \tag{1}$$

where $R(t)$ is an impulse response function and $\Gamma = 1/\tau$ is the reciprocal decay time.

It is easy to show that both the array of m points $\{t_i\}_{i=1}^m$ in which experimental data are measured and the experimental data accuracy define the interval $[\Gamma_{min}, \Gamma_{max}]$ within which the reconstruction of the distribution $P(\Gamma)$ is possible. Indeed, for any data accuracy there exists such a value Γ_{min} that for all $\Gamma < \Gamma_{min}$ the exponential $\exp(-\Gamma t)$ decays too slow to be reliably distinguished from a constant, i.e. the exponential has an infinitely small decay rate. On the other hand, there also exists a value Γ_{max} such that for $\Gamma >$

Γ_{max} the exponential $\exp(-\Gamma t)$ decays so fast that at our experimental accuracy and impulse response function $R(t)$ it cannot be distinguished from the excitation pulse.

We compute the function $P(\Gamma)$ as a histogram of n columns within the interval $[\Gamma_{min}, \Gamma_{max}]$. The bounds of the columns $\{\Gamma_j^l, \Gamma_j^h\}_{j=1}^n$ are arranged within the interval at logarithmically equal distances. The optimum for such a manner of arrangement was shown in [28]. In this case the corresponding bounds of columns at the τ-axis are arranged at logarithmically equal distances, as well.

We can compute the solution also on two additional intervals which we provisionally have called "something very fast" (SVF) and "something very slow" (SVS). The column SVF of the histogram contains all very fast components and in our calculations it was determined within the interval $[\Gamma_{n+1}^l = 100\ \Gamma_{max}, \Gamma_{n+1}^h = 500\ \Gamma_{max}]$. The column SVS of the histogram is determined within the interval $[\Gamma_{n+2}^l = 0.002\ \Gamma_{min}, \Gamma_{n+2}^h = 0.01\ \Gamma_{min}]$ and contains all components that have very slow decay rates. We can only roughly estimate the existence and the relative weights of such components by using the squares of these columns but we cannot locate their positions on Γ-axis exactly.

The above mentioned method of the discretization of eq. (1) leads to a system of m linear equations with $n + 2$ variables.

$$\mathbf{A}\boldsymbol{x} = \boldsymbol{b}, \tag{2}$$

$$\boldsymbol{b} = \left[I(t_1), \ldots, I(t_m)\right]^{\mathrm{T}}, \tag{3}$$

$$a_{ij} = \int_0^{t_i} R(t_i - t') \int_{\Gamma_j^l}^{\Gamma_j^h} \exp(-\Gamma t')\ \mathrm{d}\Gamma\ \mathrm{d}t'. \tag{4}$$

As the instrumental response function $R(t)$ is measured similar to the experimental kinetics (as a set of values $\{R_i\}$) we replace the integration over t by a summation. We furthermore introduce a set of coefficients $\{d_j\}$ that obeys the rule $d_j = (\Gamma_j^h - \Gamma_j^l)^{-1/2}$. Then we obtain:

$$a_{ij} = d_j \sum_{k=0}^{i-1} R_{i-k+1} \int_{\Gamma_j^l}^{\Gamma_j^h} \exp(-\Gamma t_k)\ \mathrm{d}\Gamma, \qquad i = 1, m; \quad j = 1, n+2, \tag{5}$$

where $t_0 = 0$. When the solution $\boldsymbol{x}$ of the system of linear equations is computed, one can find the relative weight of each column in the histogram as $h_j = x_j\ d_j$. The introduction of coefficients $\{d_j\}$ is dictated by the following reasoning. We must choose as a solution vector $\boldsymbol{x}$ which fits the experimental kinetics, within limits of accuracy of the experimental data, and in addition possesses some extreme property in the space of possible solutions. It can be shown that if we use such a method of scaling, the required extreme property will be provided by vector $\boldsymbol{x}$ of minimum Euclidean norm. Such a choice of vector $\boldsymbol{x}$ corresponds a decay rate distribution function $P(\Gamma)$ of minimum energy

$$E[P(\Gamma)] = \int P^2(\Gamma)\ \mathrm{d}\Gamma. \tag{6}$$

Indeed, using the previously obtained formulas, one can easily derive that:

$$E[P(\Gamma)] = \sum_{i=1}^{n+2} \int_{\Gamma_i^l}^{\Gamma_i^h} h_i^2\ \mathrm{d}\Gamma = \sum_{i=1}^{n+2} h_i^2(\Gamma_i^h - \Gamma_i^l) = \sum_{i=1}^{n+2} x_i^2 d_i^2(\Gamma_i^h - \Gamma_i^l) = \sum_{i-1}^{n+2} x_i^2. \tag{7}$$

Computer experiments with various rules for $\{d_j\}$ have confirmed the validity of our approach.

We use the truncated singular value decomposition (SVD) to solve the system of linear equations eq. (2) (for more details about the truncated SVD see Appendix). Unfortunately, in most cases matrix $\mathbf{A}$ is practically singular and the system eq. (2) is ill-conditioned. In this case the solution is not stable with respect to small errors in vector $\boldsymbol{b}$. Therefore, the additional stabilization of the solution is required. The requirement of the non-negativeness of the distribution given by the system of inequality constraints

$$\mathbf{G} \cdot \boldsymbol{x} \geq \boldsymbol{0}, \tag{8}$$

$$\mathbf{G} = \mathrm{diag}\{d_1, \ldots, d_{n+2}\} \tag{9}$$

strongly reduces the space of the solutions and in such a manner atabilizes the solution. We solve the problem described in eq. (2)–eq. (8) using the specially developed algorithm [29] that combines

the truncated SVD with the computation of the distribution in the presence of constraints. This algorithm is the further development of the algorithm for solving the Least Squares with Inequalities (LSI) problem [30]. Our algorithm includes the special procedure of the preliminary singularity analysis. This procedure automatically estimates the accuracy of data and fixes an optimum number of SVD components according to the level of noise. The algorithm allows the use of a single precision computer arithmetics thereby accelerating computation.

The strict mathematical description of the method of solving eqs. (2)–(8), as well as the expanded version of the program algorithm will be published separately.

The more simple algorithm for the fluorescence decay data processing based on the truncated SVD was proposed earlier [31]. This algorithm, however, provides only the three-exponential fitting of the fluorescence kinetics and has no abilities to choose an optimum number of SVD components automatically.

The described in the paper results have been computed on a 16 MHz IBM PC/AT compatible computer. The processing time is practically independent of neither the shape of the solution nor the noise level and is about five minutes.

The experimental data were measured at 255 equidistantly spaced time points in considered below examples. The function $P(\Gamma)$ was calculated within the interval $[\Gamma_{min} = 0.5/t_{max}, \Gamma_{max} = 2/t_{min}]$ which was divided into 50 logarithmically equal parts.

3.2 Decay time distribution in conditions of TDFS

After short pulse excitation, a non-equilibrium distribution over the frequency of the pure electronic transition appears in the excited state of a system with inhomogeneous broadening of electronic spectra. Nanosecond fluorescence spectrum dynamics (spectral relaxation) is observed in the system if the time of the solvate relaxation is on the order of the natural lifetime. Due to the shift of the instantaneous fluorescence spectrum the fluorescence kinetics depends on a registration frequency [32,33]. Fluorescence spectrochronogram $I(\nu, t)$ can be represented as a convolution of the solvate distribution function over the frequency of the pure electronic transition $\phi(\nu, t)$ (inhomogeneous broadening function, IBF) and the homogeneous fluorescence spectrum $S(\nu)$:

$$I(\nu, t) = i_0 \exp(-t/\tau_0) \int_{-\infty}^{+\infty} \phi(\nu', t) S(\nu - \nu')\, d\nu', \tag{10}$$

where τ_0 is a natural lifetime of the excited state, ν' is a frequency of the pure electronic transition and i_0 is a constant (we will assume $i_0 = 1$ for the sake of simplicity).

The equilibrium IBF of the polar dye solution has a Gaussian shape [33]:

$$\phi(\nu, t) = \frac{1}{\sqrt{2\pi}\,\sigma(t)} \exp\left(- \frac{[\nu - \nu_0(t)]^2}{2\sigma^2(t)} \right). \tag{11}$$

The temporal transformation of IBF as it was shown [25,34] can be defined as follows:

$$\nu_0(t) = \nu_0(\infty) + \Delta\nu(\beta_1 \exp(-t/\tau_1) + \beta_2 \exp(-t/\tau_2)), \tag{12}$$

for $\beta_1, \beta_2 \geq 0$ and $\beta_1 + \beta_2 = 1$,

$$\sigma(t) = \sigma(\infty) + \Delta\sigma \exp(-t/\tau_3). \tag{13}$$

This model phenomenologically correctly describes the shift of the fluorescence spectrum and the changes of the width of the spectrum.

The problem with theoretical calculations of DTD is reduced to the inverse Laplace transform $P(\nu, \Gamma) = \mathcal{L}^{-1}(I(\nu, t))$ of the fluorescence kinetics $I(\nu, t)$. In other words, $P(\Gamma)$ can be obtained as a solution of the equation:

$$I(\nu, t) = \int_0^{\infty} P(\nu, \Gamma) \exp(-\Gamma t)\, d\Gamma. \tag{14}$$

If $I(\nu, t)$ is given by eq. (10) it is easy to show that the inverse Laplace transform of the kinetics is expressed as follows:

$$P(\nu, \Gamma) = \int_{-\infty}^{+\infty} \mathcal{L}^{-1}(\exp(-t/\tau_0)\phi(\nu', t)) \times S(\nu - \nu')\, d\nu'. \tag{15}$$

By this way the form of DTD is defined by the inverse Laplace transform of IBF.

Expanding IBF (eq. 11) in a series and taking into account eqs. (12) and (13) one obtains:

$$P(\nu,\Gamma)=\sum_{i=0}^{\infty}A_i\delta\left(\Gamma-\frac{1}{\tau_0}-\frac{i}{\tau_9}\right)+\sum_{i=0}^{\infty}\sum_{j=0}^{i}\sum_{k=1}^{\infty}\sum_{n=0}^{2k}\sum_{m=0}^{n}A_iB_{jknm}(\nu)\times\delta\left(\Gamma-\frac{1}{\tau_0}-\frac{n-m}{\tau_1}-\frac{m}{\tau_2}-\frac{i}{\tau_3}\right), \tag{16}$$

where

$$A_i=\left(-\frac{\Delta\sigma}{\sigma(\infty)}\right)^i, \tag{17}$$

$$B_{jknm}(\nu)=\int_{-\infty}^{+\infty}B'_{jknm}(\nu')S(\nu-\nu')\,d\nu', \tag{18}$$

$$B'_{jknm}(\nu)=(-1)^{k+n}\frac{2(2k+j-1)!}{j!m!(k-1)!(n-m)!(2k-n)!}\beta_1^{n-m}\beta_2^m\times\left(\frac{\Delta\nu}{\sqrt{2}\sigma(\infty)}\right)^n\left(\frac{\nu-\nu_0(\infty)}{\sqrt{2}\sigma(\infty)}\right)^{2k-n}. \tag{19}$$

Here we assume that

$$\int_{-\infty}^{+\infty}S(\nu)\,d\nu=1. \tag{20}$$

We can see from eq. (16) that the DTD under conditions of single- or double-exponential TDFS is discrete, i.e. not a continuous one as, for example, the DTD under conditions of Förster (radiationless) energy transfer (see, e.g., [4,22]). The shape of the homogeneous spectrum $S(\nu)$ affects only the relative weights of δ-functions. Therefore, we can state that for any system in which the spectral relaxation according to the above described model takes place, the DTD will be discrete, independent of (homogeneous) spectrum shape. Positions of the δ-functions will depend only on the characteristic times of the spectral relaxation.

It should be noted that when DTD is represented by closely spaced δ-functions the weights of which are approximately equal or monotonously increase or decrease, we deal with the so-called "quasi-continuous" distribution. This means that in practice the limited temporal resolution and noise in data will not allow recovery of the structure of the DTD, so that it will be treated as a continuous one. (This is the common way of simulating continuous distributions.) In contrast, there may be a situation when δ-functions in discrete DTDs are gathered in several well-spaced groups. In such a case we obtain the "quasi-discrete" DTD. It means that one cannot resolve experimentally the structure of these groups, but instead obtain well-spaced rather broad peaks.

Therefore it will be useful to analyze the structure of the obtained DTD. Considering eq. (16) one can determine DTD structure. We can see that this distribution consists of a separately located δ-function at τ_0 and, at lower decay times, sequences of δ-functions for each τ_i ($\delta(\Gamma-(1/\tau_0)-(n/\tau_i))$, $n=1,\infty$) where $i=1,2,3$ and, lastly, a complex result of the "interference" of these sequences ($\delta(\Gamma-(1/\tau_0)-(i/\tau_1)-(j/\tau_2)-(k/\tau_3)$, $(i,j,k)=0,\infty$, excluding those cases when two or three indices simultaneously equal zero). Note that the decay time distribution always lies within the interval $\tau\in[0,\tau_0]$, irrespectively of values of τ_i.

It is clear that each of these three sequences appears at decay time

$$\tau_i^{\dagger}=\frac{\tau_0\tau_i}{\tau_0+\tau_i},\quad i=1,2,3 \tag{21}$$

and lasts towards lower decay times. The weights of δ-functions of each sequence are represented by a convergent series and therefore after a finite number of terms of the sequence the weights of the δ-functions become negligibly small. Therefore, each sequence can be characterized by some mean decay time. However, the weights of the δ-functions in the sequence depend on the emission frequency (eq. 9) and therefore the mean time of a sequence too.

Computations have shown that the in the present paper considered cases of DTD's for TDFS-systems are "quasi-discrete" (Section 4.3). It will be shown in Sections 4.3 and 4.4 that this "quasi-

discreteness" of DTD's of TDFS-systems can be successfully applied to analyse fluorescent probe dynamics.

4. Results and discussion

4.1 Computer simulations

We have investigated the abilities of our algorithm to recover the DTD from the fluorescence kinetics at low level of precision conditions (CPC = 5 10^3) by means of computer simulations.

The fluorescence kinetics corresponding to a given DTD was convolved with the excitation pulse (flash-lamp) with CPC = 5 10^9. The width of the response function at the half of its maximum was about 2 ns. Data consisted of 255 channels with 0.16 ns per channel. A typical simulated decay curve as well as the corresponding excitation pulse ar shown in Fig. 1.

The examples of the recovery of single-exponential decays for various decay times are presented in Fig. 2.

The recovery of the double-exponential process obviously depends (at fixed data accuracy) on the separation of the decay times (Fig. 3). We can take into account *a priori* information about the system. In the ideal case the DTD consists of discrete exponential δ-functions. Therefore, we can compute in this case the "sharpened" solution. This is equivalent to the choice of a greater number of SVD components than that chosen automatically based on the noise level. We can see that using such an operation one can suffi-

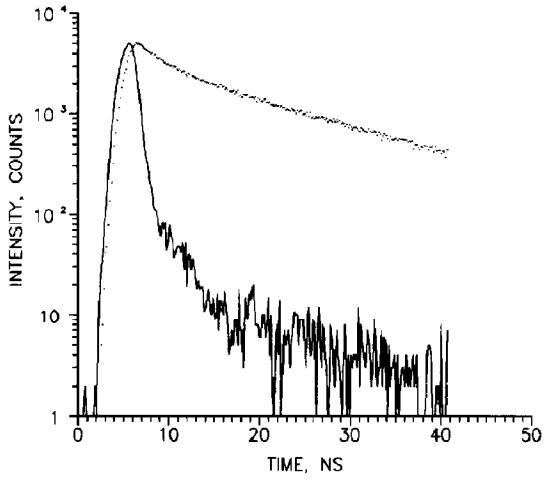

Fig. 1. The stimulated fluorescence kinetics (dotted line) for the three-exponential decay with the parameters similar to the case of Fig. 4(a) convolved with the real excitation pulse of the flash-lamp (solid line).

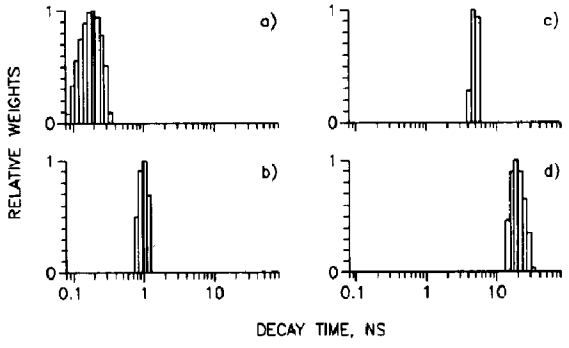

Fig. 2. The recovery of the single-exponential decays. CPC = 5 10^3, 255 channels, 0.16 ns/ch. (a) $\tau = 0.2$ ns, (b) $\tau = 1$ ns, (c) $\tau = 5$ ns, and (d) $\tau = 20$ ns.

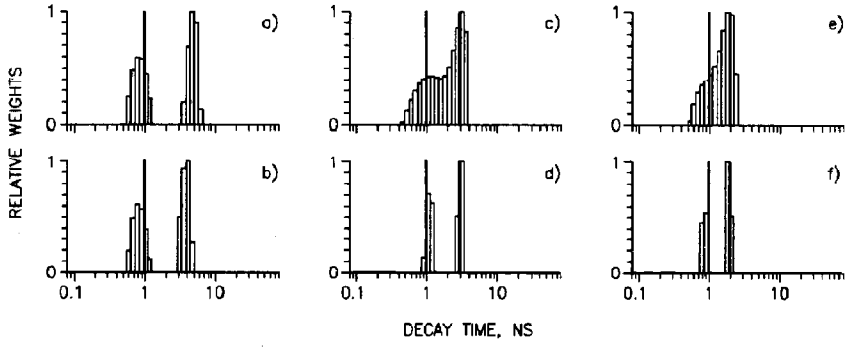

Fig. 3. The recovery of double-exponential decays as a function of the separation. $r = \tau_2/\tau_1$. CPC = 5 10^3, 255 channels, 0.16 ns/ch. (a) $r = 5$; (b) $r = 4$; (c) $r = 3$; (d) $r = 3$, "sharpened" solution; (e) $r = 2$; and (f) $r = 2$, "sharpened" solution.

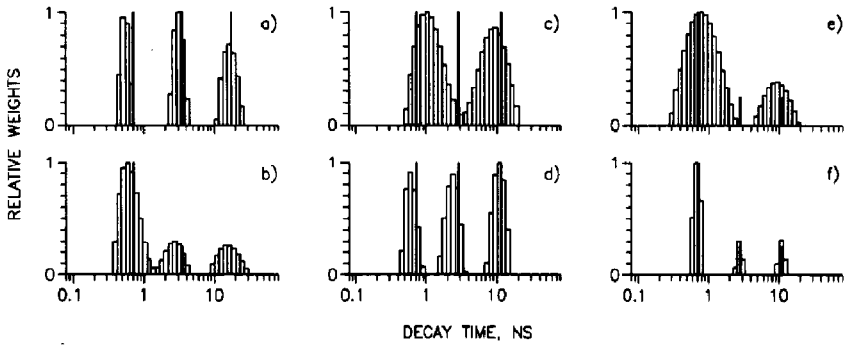

Fig. 4. The recovery of three-exponential decays as a function of separation and relative weights. $r = \tau_3/\tau_2 = \tau_2/\tau_1$. CPC = 5 10^3, 255 channels, 0.16 ns/ch. (a) $r = 5$, $c_1 : c_2 : c_3 = 1 : 1 : 1$; (b) $r = 5$, $c_1 : c_2 : c_3 = 4 : 1 : 1$; (c) $r = 4$, $c_1 : c_2 : c_3 = 1 : 1 : 1$; (d) the same as (c), "sharpened" solution; (e) $r = 4$, $c_1 : c_2 : c_3 = 4 : 1 : 1$; (f) the same as (e), "sharpened" solution.

ciently improve the temporal resolution (Fig. 3c, d and e, f). Nevertheless, it should be noted that this method should be used only if we know that the fluorescence kinetics consists of discrete exponential decays.

The examples of the recovery of three-exponential decays with various relative weights and separations are presented in Fig. 4. As in previous case the recovery of DTD critically depends on the separation of decay times.

The ability to recover the shape of the continuous distribution was tested using the lognormal distributions of decay times (Fig. 5). It is clear that "fast" components are cut off because of both the convolution of the real kinetics with wide response function and the noise level in the data.

We have found that because of the non-negative constraints (Section 3.1) our method provides stable recovery of the positive part of the DTD in the presence of strong negative components at short decay times. The resolution of discrete decays is certainly worse in this case (Fig. 6).

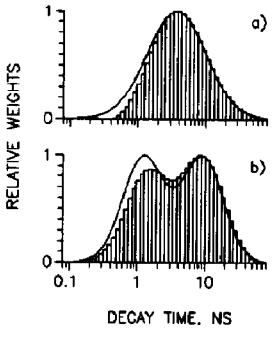

Fig. 5. The recovery of the unimodal (a) and bimodal (b) lognormal distributions. CPC = 5 10^3, 255 channels, 0.16 ns/ch.

4.2 DTD for dye solutions with exponential decays

We have tested our program also by studying the fluorescence decays of liquid dye solutions (n-propanol at the room temperature). Since the

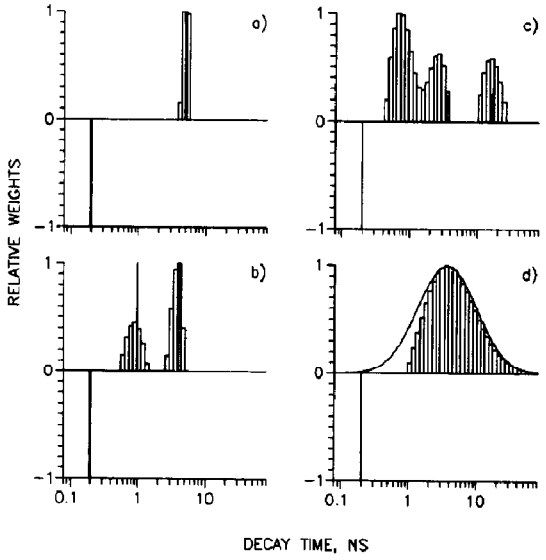

Fig. 6. The recovery of the positive parts of DTD in the presence of the exponential with the negative pre-exponential factor. CPC = 5 10^3, 255 channels, 0.16 ns/ch. The parameters of the positive part of DTD are: (a) as in Fig. 2(c); (b) as in Fig. 3(b); (c) as in Fig. 4 (b); (d) as in Fig. 5 (a).

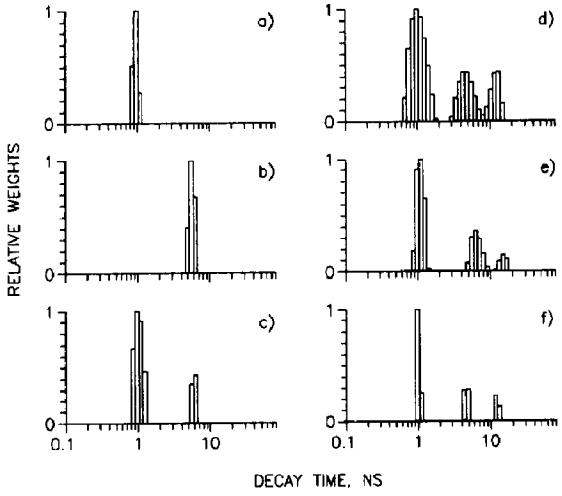

Fig. 7. Decay time distributions for solutions of non-interacting fluorophores with exponential decays in n-propanol, $T = 22°C$, $\nu_{ex} = 29740\ cm^{-1}$, $\nu_{em} = 23800\ cm^{-1}$; 255 channels, 0.32 ns/ch; (a) *p*-quaterphenyl (CPC = $5\ 10^3$); (b) 1-AN (CPC = $3\ 10^3$); (c) *p*-quaterphenyl + 1-AN (CPC = $1.4\ 10^4$); (d) *p*-quaterphenyl + 1-AN + 3-ANMP (CPC = $3\ 10^3$); (e) *p*-quaterphenyl + 1-AN + 3-ANMP (CPC = $1.4\ 10^4$); (f) the same as (d), "sharpened" solution.

solvate relaxation time of n-propanol at room temperature lies in the picosecond region the decays of the single-component solutions are exponential (Fig. 7a, b).

We have recovered DTD's for mixtures of two and three non-interacting chromophores (Fig. 7c, d). The recovered lifetimes are in good coincidence with those obtained in cases a, b. The width of a peak allows an estimation of the accuracy of the measured decay time value. The increase in the accuracy of data leads to the decrease in the widths of DTD peaks (Fig. 7e).

We can take into account *a priori* information about our system and compute the "sharpened" solution (see Section 4.1). The results of such an analysis are represented in Fig. 7(f). We can see in this case that the choice for a greater number of SVD components sufficiently increases the accuracy of the experimental data. Still, we must once more emphasize that such a "method of improving accuracy" should be applied only in those cases when we do know that the experimental kinetics consists of several (two or three) discrete exponential decay functions.

4.3 Decay time distribution for TDFS-systems

The dependence of the fluorescence kinetics of the solution of 3-ANMP in glycerol both on the emission and the excitation frequencies has been examined earlier [35]. It has been found that the model of the inhomogeneous broadening (field diagram) makes it possible to describe qualitatively the fluorescence kinetics both at blue and red slopes of the emission spectrum. The fluorescence kinetics under conditions of TDFS depends on the evolution of IBF and the registration frequency in accordance with eq. (10).

For the simplification of the theoretical calculations we have used a more simple form of model eq. (10). Instead of the real instantaneous spectrum we chose the Gaussian with moving center of gravity and altering width. The fluorescence kinetics in this case is as follows:

$$I(\nu, t) = i_0 \exp(-t/\tau_0) \frac{1}{\sqrt{2\pi}\,\sigma(t)} \times \exp\left(-\frac{[\nu - \nu_0(t)]^2}{2\sigma^2(t)}\right), \qquad (22)$$

where $\nu_0(t)$ and $\sigma(t)$ are as defined in Section 3.2. This model can be used for the description of the fluorescence kinetics at the blue slope of the emission spectrum.

The parameters of the model (the spectral shift range $\Delta\nu$, spectrum width σ, its altering in during spectral relaxation ($\Delta\sigma$, τ_3) and the spectral shift law (β_1, β_2, τ_1, τ_2)) were estimated in the first stage of the calculations on the basis of time-resolved emission spectra (zero approximation) and then were more accurately defined by using a non-linear fitting (Nelder–Mead algorithm) of the model emission kinetics to that experimentally found. (3-ANMP in glycerol, $\nu_{ex} = 27900\ cm^{-1}$, $\nu_{em} = 25000\ cm^{-1}$).

The theoretical DTD for the simplified model (eq. 22) is shown in Fig. 8(a). It was calculated using previously defined spectral shift parameters. A δ-function corresponds to the infinitely high temporal resolution of the fluorometre, but since this is not a real situation, the distributions were computed in the form of histograms with

the parameters described in Section 3.1. In this situation the weight of a bar represents the sum of weights of δ-functions taken in linear Γ-scale within the bar interval.

Numerically computed DTD for the simulated (eq. (22) and the experimental kinetics are represented in Fig. 8(b), (c). We can see that DTD recovered both from the simulated and the experimental kinetics consist of three peaks whose positions correlate with the ones of the sequences of the δ-functions of the theoretical distribution.

If we fix the excitation frequency and decrease the registration (emission) frequency so that it stays within limits of the blue slope of the emission spectrum, we obtain a relative decrease of weights of "fast" components in the DTD. This can be explained by the next speculations. Let us consider the decrease of the fluorescence intensity caused by the spectral shift only. Then, if the registration point at the time zero is located closely to the maximum of the spectrum, the decrease of the intensity is smaller than if the registration point was at the blue wing (provided that the spectrum shifts towards the red region). This circumstance is caused by using a Gaussian-like spectrum shape.

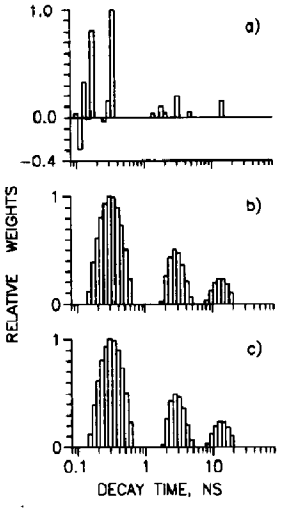

Fig. 8. Decay time distributions for 3-ANMP in glycerol, $[C] = 5\ 10^{-5}$ M, $T = 22°C$, $\nu_{ex} = 27900$ cm^{-1}, $\nu_{em} = 25000$ cm^{-1}; 255 channels, 0.16 ns/ch; (a) theoretical (eq. 16); (b) computed from simulated kinetics (eq. 22); (c) computed from experimental kinetics (CPC = $5\ 10^3$).

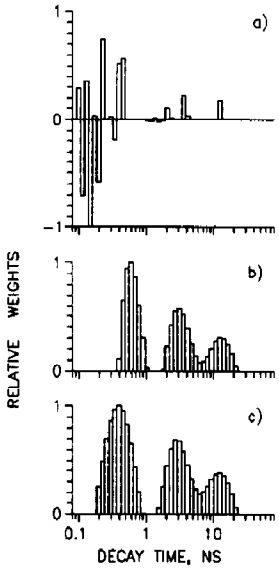

Fig. 9. Decay time distributions for 3 ANMP in glycerol, $[C] = 5\ 10^{-5}$ M, $T = 22°C$, $\nu_{ex} = 27900$ cm^{-1}, $\nu_{em} = 22200$ cm^{-1}; 255 channels, 0.16 ns/ch; (a) theoretical (eq. 16); (b) computed from simulated kinetics (eq. 22); (c) computed from experimental kinetics (CPC = 10^4).

Similar to the previous case, the results for a registration frequency of 22200 cm^{-1} are shown in Fig. 9. The presence of strong negative components in the theoretical DTD is caused by the fact that the registration point is located at the red slope of the instantaneous emission spectrum at zero time. As the first stage of the relaxation occurs with high rate, the negative components appear at short decay times.

It should be noted that the width of relaxation time τ_3 appeared to be close to its value found with longer relaxation times. Therefore, only two peaks connected with the spectral relaxation are observed in the distributions.

The magnitude of the spectral shift decreases at the red-edge excitation [36]. We have investigated the character of the fluorescence kinetics at an excitation frequency of 23250 cm^{-1} using the same registration frequency as in the case represented in Fig. 9. Using our model (eq. 22) we found that in this case the spectral shift region is about 500 cm^{-1}, which is sufficiently smaller than the one with excitation at the maximum of the absorption spectrum (2700 cm^{-1}). Moreover, the

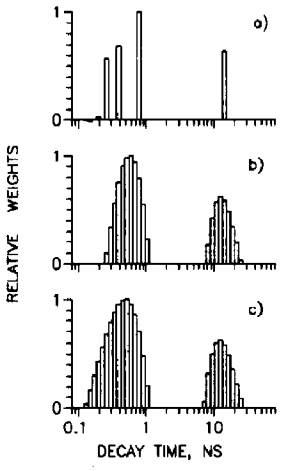

Fig. 10. Decay time distributions for 3-ANMP in glycerol, $[C]=5\ 10^{-4}$ M, $T=22°C$, $\nu_{ex}=27900\ cm^{-1}$, $\nu_{em}=25000\ cm^{-1}$; 255 channels, 0.16 ns/ch; (a) theoretical (eq. 16); (b) computed from simulated kinetics (eq. 22); (c) computed from experimental kinetics (CPC = $3\ 10^3$).

width of the time-resolved emission spectrum practically does not alter in the process of the spectral relaxation and is practically equal to one of the relaxed spectrum at the excitation at the maximum of absorption. Instead of the double-exponential shift, as in previous case ($\tau_1=0.45$ ns, $\tau_2=4.8$ ns, $\beta_1/\beta_2=0.72/0.28$), we now have a single-exponential shift with $\tau_1=1.2$ ns.

Figure 10 shows the theoretical, the simulated and the experimental DTD for the red-edge excitation. As expected the weight of the fast components decreased. The experimentally obtained DTD in this case contains only one peak connected with the spectral relaxation. This fact is in good agreement with the assumption of the mono-exponential character of the spectral shift.

We can estimate the values of τ_1 and τ_2 using in eq. (21) instead of $\tau_i^{\dagger}$ the centers of gravity of relaxation peaks τ_i^G of the experimentally obtained distribution. The estimated values of τ_1 and τ_2, as well as the weights of DTD peaks P_0, P_1, P_2 are listed in Table 1.

Our investigations make it possible to explain the emission frequency dependence of the parameters recovered by the three-exponential fitting of the fluorescence kinetics in systems with TDFS (see, e.g., [33]). As discussed in Section 3.2, the mean decay times of the sequences of the distribution depend on the registration frequency. The three-exponential fitting allows to recover some mean parameters of the fluorescence kinetics of such systems. Therefore, one can suppose that these mean parameters correspond to those of the above described sequences. In this way, it is clear that the parameters of the three-exponential model should depend on the emission frequency.

4.4 DTD for probes 1-AN and 2,6-TNS in membranes

We investigated fluorescence DTD for 1-AN and 2,6-TNS probes incorporated into phosphatidylcholine bilayer membranes. From [37] it is known that 1-AN and 2,6-TNS probes possess electrical dipole moments that increase after optical transition from the S_0 to S_1 state. Owing to the presence of a negatively charged sulfate group, the 2,6-TNS probes locate in the region of the heads of phospholipids at the polar surface layer of the membrane phospholipide bilayer. Nonionic 1-AN probes can penetrate into the bilayer more deeply and locate on the level of the glycerol skeleton and the carbonyl group of the phospholipids. Thus, both probes are located in the

Table 1

Fluorescence DTD analysis for 3-ANMP in glycerol

Excitation frequency (cm^{-1})	Registration frequency (cm^{-1})	Centers of gravity of peaks (ns)			Estimated relaxation times (ns)		Relative weights of peaks		
		τ_0^G	τ_1^G	τ_2^G	τ_1	τ_2	P_0	P_1	P_2
27900	22500	12.0	2.9	0.4	3.4	0.4	0.12	0.21	0.67
27900	22200	12.6	3.3	0.6	4.5	0.6	0.19	0.34	0.47
23250	22200	13.6	0.5	–	0.5	–	0.28	0.72	–

polar region of the bilayer. The inhomogeneous broadening of fluorescence spectra has been found and studied for these probes both in viscous polar solution and membranes [38,39]. The time-resolved emission spectra show nanosecond dynamics with temperature-dependent rates.

As shown in Section 3.2, the information about the law of the spectral shift is contained in the fluorescence kinetics of polar dye solutions. Therefore, we can except that our method allows us to study the dynamic properties of the polar part of the membrane.

The DTD's for 1-AN in membranes at the excitation in the maximum of absorption and registration on the blue slope of the emission at three different temperatures: 22°C, 14°C and 8°C are shown in Figs. 11a–c. The results of the DTD analysis for these cases are listed in Table 2.

It can be seen that in all three cases the distributions consist of discrete peaks. As it is clear from the previous considerations (Section 3.2), the right peak is connected with the natural lifetime, whereas the other peaks depend on the spectral shift. Therefore, the positions and relative weights of the last have to depend on the temperature. The independence of the right peak position from temperature (in experimental accuracy limits) gives evidence that the natural lifetime does not depend on the probe's environment microviscosity. (The position of the peak corresponding to τ_0 can be found more precisely by using the "sharpened" solution; in this case $\tau_0 = 7.2 \pm 0.8$ ns.) The decrease of the temperature makes the spectral shift more slow. This has to lead to a decrease in the relative weights of the fast components of the DTD. One can notice that

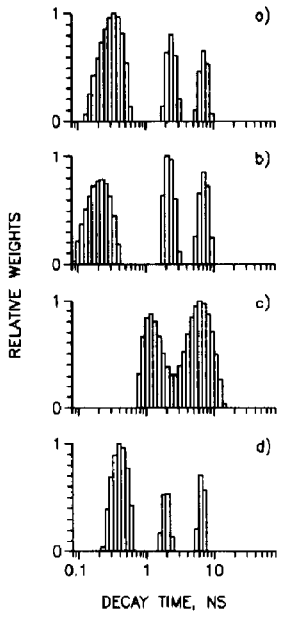

Fig. 11. Decay time distributions for 1-AN (a, b, and c), and 2,6-TNS (d) in model membranes, $\nu_{ex} = 27900\ cm^{-1}$, $\nu_{em} = 25000\ cm^{-1}$; 255 channels, 0.16 ns/ch; (a) $T = 22°C$ (CPC = $2.5\ 10^3$); (b) $T = 14°C$ (CPC = 10^4); (c) $T = 8°C$ (CPC = 10^4); (d) $T = 14°C$ (CPC = $5\ 10^3$).

at 8°C, the fast component of DTD for 1-AN is not resolved such that it can be connected with a decrease in the relative weight of the fast component.

On the basis of the obtained DTD we can estimate the mean time of the spectral shift $\langle \tau_R \rangle = (P_1\tau_1 + P_2\tau_2)/(P_1 + P_2)$. It was found that this parameter monotonously decreases with an increase in temperature (see Table 2).

Table 2

Fluorescence DTD analysis for 1-AN and 2,6-TNS in bilayer phosphatidylcholine membranes

Probe	Temperature (°C)	Centers of gravity of peaks (ns)			Estimated relaxation times (ns)		Relative weights of peaks			Estimated mean time of spectral shift $\langle \tau_R \rangle = \frac{P_1\tau_1 + P_2\tau_2}{P_1 + P_2}$ (ns)
		τ_0^G	τ_1^G	τ_2^G	τ_1	τ_2	P_0	P_1	P_2	
1-AN	8	6.3	1.3	–	1.6	–	0.60	0.40	–	1.6
	14	7.3	2.3	0.2	3.4	0.2	0.23	0.27	0.50	1.3
	22	7.2	2.4	0.3	3.6	0.3	0.16	0.21	0.64	1.1
2,6-TNS	14	6.5	1.9	0.4	2.7	0.4	0.19	0.17	0.64	0.9

DTD for probe 2,6-TNS in membrane also constraints of discrete peaks (Fig. 11d) at the excitation in the maximum of the absorption and at blue-slope registration. The similar character of DTD for both probes shows that in these two cases we deal with the same phenomenon of dipole–dipole relaxation. In accordance with the well known fact that the microviscosity is greater in the region of the glycerol skeleton than in the region of phospholipide heads [37], the mean time of the spectral shift $\langle \tau_R \rangle$ for 2,6-TNS is found smaller than that for 1-AN at the same temperature.

5. Conclusions

The described method of recovery of decay time distributions by means of a truncated singular value decomposition and the computation of the solution in presence of constraints allows interpretation of complex fluorescence kinetics. The method enables us to differentiate with confidence up to three exponential processes at relatively low level of experimental accuracy (5 10^3 CPC) the characteristic decay times which differ in magnitude by about a factor of four to five.

We have found that in the case when the spectral relaxation can be represented as a single- or double-exponential shift of the emission spectrum, the decay time distribution of a system with TDFS consists of a single well-separated δ-function at τ_0 and several sequences of closely spaced δ-functions. At some combinations of values of the parameters of the spectral shift, these sequences are located separately and their positions can be recovered from the fluorescence kinetics.

In such a manner it is possible to estimate the relaxation constants of the spectral shift from the kinetics measured at the blue slope ends of the emission spectrum. The investigation of the spectral relaxation of the electronic spectra of polar dye solutions is quite interesting for both creation of the theory of polar solutions and study of the dynamics of biochemical samples. It is particularly important that our method enables estimation of the dynamic characteristics of polar solutions under conditions of low experimental accuracy level (5 10^3–5 10^4 CPC). It renders the method attractive for studying the dynamic properties of the biochemical microsamples, since the experimental accuracy cannot be improved in this case due to low concentration or photochemical destruction of probes.

Acknowledgement

The authors would like to thank Dr. N.V. Shcherbatska for her help in the preparation of biochemical samples.

Appendix

The truncated singular value decomposition principle

We use the truncated singular value decomposition (SVD) to stabilize the solution of our overdetermined but nevertheless ill-conditioned (i.e. unstable) system of m linear equations with n variables:

$$\mathbf{A}\boldsymbol{x} = \boldsymbol{b} \tag{A.1}$$

SVD of matrix $\mathbf{A}$ is defined as

$$\mathbf{A} = \mathbf{U}\mathbf{S}\mathbf{V}^{\mathrm{T}} \tag{A.2}$$

where $\mathbf{U}_{m\times n}$ and $\mathbf{V}_{n\times n}$ are orthogonal matrices and $\mathbf{S}_{n\times n}$ is the diagonal matrix with the so-called singular numbers on the main diagonal. Having the decomposition and using the properties of the orthogonal matrices:

$$\mathbf{U}^{\mathrm{T}}\mathbf{U} = E_n,$$
$$\mathbf{V}^{\mathrm{T}}\mathbf{V} = \mathbf{V}\mathbf{V}^{\mathrm{T}} = E_n \tag{A.3}$$

one can easily compute the least squares solution of the original system as:

$$\boldsymbol{x} = \mathbf{V}\mathbf{S}^{-1}\mathbf{U}^{\mathrm{T}}\boldsymbol{b}$$
$$\mathbf{S}^{-1} = \mathrm{diag}\{1/s_1, \ldots, 1/s_n\}. \tag{A.4}$$

The only problem might occur (and it does in our case) that some of the singular numbers are zero (or practically zero from a computational

point of view) or relatively very small. Zero singular numbers do not allow us to compute the inverse to the matrix **S**. The principle of truncated SVD prescribes us to cope with this problem by putting the corresponding elements of $\mathbf{S}^{-1}$ to zero. It may be shown that such an operation provides the least squares solution of minimum Euclidean norm. Small singular numbers allow a solution to exist but their reverse values in eq. (A.4) dramatically increase errors in the input vector $\boldsymbol{b}$ making the solution intolerable. Going further with the truncated SVD we choose some threshold η by replacing some elements of $\mathbf{S}^{-1}$ by zeros:

$$s_i^{-1} = \begin{cases} 1/s_i, & s_i > \eta \\ 0, & s_i \le \eta \end{cases} \qquad \text{(A.5)}$$

A large threshold will increase the residual norm but reduce the solution norm making the solution more stable (and coarser).

For most of the problems it is possible to find a trade-off so that both of these norms will be small enough. The way of how we do that and how we force the solution to be non-negative will be published in a forthcoming, more mathematical, paper.

References

1 D.V. O'Connor, W.R. Ware and J.C. Andre, J. Phys. Chem. 83 (1979) 1333.
2 D.R. James and W.R. Ware, Chem. Phys. Lett. 126 (1986) 7.
3 A.K. Livesey and J.C. Brochon, Biophys. J. 52 (1987) 693.
4 A. Siemiarzcuk, B.D. Wagner and W.R. Ware, J. Phys. Chem. 94 (1990) 1661.
5 J.R. Lakowicz, H. Cherek, I. Gryczinsky, M.L. Johnson and N. Joshi, Biophys. Chem. 28 (1987) 35.
6 I.R. Alcala, E. Gratton and F.G. Prendergast, Biophys. J. 51 (1987) 567.
7 T. Parasassi, F. Conti, E. Gratton, Chem. Phys. Lett. 898 (1987) 7.
8 R.M. Fiorini, E. Bertoli, G. Curattola, E. Gratton and M. Valentino, Biochem. Biophys. Res. Commun. 147 (1987) 460.
9 D.R. James, J.R. Turnbul, W.D. Wagner and N.O. Petersen., Biochem. 26 (1987) 6272.
10 R. Fiorini, M. Glaser, E. Gratton et al., Biochem. 26 (1987) 3864.
11 J.R. Alcala, E. Gratton and F.G. Prendergast, Biophys. J. 51 (1987) 925.
12 J.R. Alcala, E. Gratton and F.G. Prendergast, Biophys. J. 51 (1987) 597.
13 B.D. Wagner, D.R. James and W.R. Ware, Chem. Phys. Lett. 138 (1987) 181.
14 A. Siemiarzcuk and W.R. Ware, J. Phys. Chem. 91 (1987) 3677.
15 R.M. Fiorini, M. Valentino, M. Glaser, E. Gratton and G. Curattola, Biochim. Biophys. Acta. 939 (1988) 485.
16 B.W. Williams and C.D. Stibbs, Biochemistry 27 (1988) 7994.
17 R.M. Fiorini, E. Gratton and G. Curattola, Biochem. Biophys. Acta. 1006 (1989) 198.
18 M.L. Wratten, E. Gratton, A. Sevanian and M. van der Ven, Biochem. Biophys. Res. Commun. 164 (1989) 169.
19 E. Kalb, F. Paltauf and A. Germetter, Biophys. J. 56 (1989) 1245.
20 A. Siemiarzcuk and W.R. Ware, J. Phys. Chem. 93 (1989) 7609.
21 M. Gentin, M. Vincent, J.C. Brochon, A.K. Livesey, N. Cittanova and J. Gallay, Biochem. 29 (1990) 10405.
22 B.D. Wagner and W.R. Ware, J. Phys. Chem. 94 (1990) 3489.
23 D.R. James and W.R. Ware, J. Phys. Chem. 94 (1985) 455.
24 W.R. Ware, G.J. Brant and P.P. Chow, J. Chem. Phys. 54 (1971) 4729.
25 D.M. Gakamsky, N.A. Nemkovich, A.N. Rubinov. Izv. AN SSSR, ser. fiz. (USSR) 64 (1989) 2396.
D.M. Gakamsky, N.A. Nemkovich, A.N. Rubinov and V.I. Tomin. J. Mol. Liq. 45 (1990) 33.
26 1-AN was synthesized at the Institute of Organic Chemistry of Ukrainian Academy of Sciences, Kiev
27 D.M. Small and M.C. Bourger, Biochim. Biophys. Acta 125 (1966) 563.
28 N. Ostrovsky, D. Sormette, P. Parker and E.R. Pike, Optica Acta 28 (1981) 1059.
29 A.A. Goldin, Solving ill-conditioned systems of linear equation with constraints. (Preprint No. 22. NTO AN SSSR, Leningrad, 1989); A.A. Goldin and T.D. Brygina, A program system for exponential and Lorenzian decay curves decomposition (Preprint No. 26. NTO AN SSSR, Leningrad, 1989).
30 C.L. Lawson and R.J. Henson, Solving least squares problems (Prentice-Hall, Englewood Cliffs, NJ, 1974).
31 G. Striker, in: Deconvolution and reconvolution of analytical signals, ed. M. Bouchy (University Press, Nancy, 1982) p. 329.
32 N.A. Nemkovich, V.I. Matseiko and V.I. Tomin, Opt. Spektr. (USSR) 49 (1980) 274.
33 R.P. DeToma, J.H. Easter and L. Brand, J. Am. Chem. Soc. 16 (1976) 5001.
34 A.N. Rubinov and V.I. Tomin, Inhomogeneous broadening of electronic spectra of organic molecules in solid and liquid solutions (Preprint No. 348, Institute of Physics BSSR Acad. of Sci., Minsk, 1984).
35 D.M. Gakamsky, N.A. Nemkovich and A.N. Rubinov, Zhurn. Prikl. Spektr. (USSR) 54 (1991) 183.

36 N.A. Nemkovich, V.I. Matseiko, A.N. Rubinov and V.I. Tomin, Opt. Spektr. (USSR) 29 (1979) 780.
37 Yu.A. Vladimirov and G.E. Dobretsov, Fluorescent probes in the study of biological membranes (Nauka, Moscow, 1980).
38 D.M. Gakamsky, A.P. Demchenko, N.A. Nemkovich, A.N. Rubinov, B.I. Tomin and N.V. Shcherbatska, Time-resolved laser spectroscopy of 1-AN probe in phospholipid membranes (Preprint No. 487 Institute of Physics BSSR Acad. of Sci., Minsk, 1987).
39 A.P. Demchenko and N.V. Shcherbatska, Biophys. Chem. 22 (1985) 131.